SCIENCE CHINA
Information Sciences

• RESEARCH PAPER •

June 2022, Vol. 65 162405:1–162405:9
https://doi.org/10.1007/s11432-021-3360-0

A low-fabrication-temperature, high-gain chip-scale waveguide amplifier

Bo WANG[1], Peiqi ZHOU[1,2], Xingjun WANG[1,3,4,5*] & Yandong HE[2]

[1]*State Key Laboratory of Advanced Optical Communication Systems and Networks, Department of Electronics, School of Electronics Engineering and Computer Science, Peking University, Beijing* 100871*, China;*
[2]*Institute of Microelectronics, School of Electronics Engineering and Computer Science, Peking University, Beijing* 100871*, China;*
[3]*Frontier Science Center for Nano-optoelectronics, Peking University, Beijing* 100871*, China;*
[4]*Peking University Yangtze Delta Institute of Optoelectronics, Nantong* 226010*, China;*
[5]*Peng Cheng Laboratory, Shenzhen* 518055*, China*

Received 14 July 2021/Revised 22 August 2021/Accepted 28 October 2021/Published online 19 May 2022

Abstract The increasing prevalence of integrated on-chip optoelectronic devices has identified serious issues regarding inter-device transmission and coupling losses, highlighting an urgent need for on-chip waveguide amplifiers to compensate for these losses. Compared with other Er-based optical materials, erbium silicate is ideally suited to high-efficiency on-chip amplifiers and lasers because of its extremely high Er^{3+} concentration (10^{22} cm^{-3}). Nevertheless, erbium silicate must be annealed above 1000°C to crystallize and activate the Er^{3+}, which damages other on-chip optoelectronic components and is not conducive to device integration. Here, we report a low-fabrication-temperature, high-luminescence-efficiency gain material by adding Bi_2O_3 to an erbium-ytterbium silicate mixed film. Our experiments demonstrate that the proposed film crystallizes at 600°C while the activation of Er^{3+} is also achieved, which is the lowest activation temperature of on-chip waveguide amplifier to our knowledge. This material forms the basis for a new chip-scale waveguide amplifier design, with a theoretical multi-energy-level model of Bi-Er-Yb in the mixed thin films used to analyze its signal enhancement properties. We achieve a peak on-chip gain of 23 dB in a 3.3-mm-long waveguide under the pump and signal powers of 300 mW and 1 μW, respectively. These results highlight the potential of the proposed material for realizing on-chip amplifiers and lasers for large-scale nanophotonic integrated circuits.

Keywords photonic circuit integration, low fabrication temperature, high gain, rare earth material, waveguide amplifier

Citation Wang B, Zhou P Q, Wang X J, et al. A low-fabrication-temperature, high-gain chip-scale waveguide amplifier. Sci China Inf Sci, 2022, 65(6): 162405, https://doi.org/10.1007/s11432-021-3360-0

1 Introduction

In light of the rapid development of on-chip optical communication technology and the continuous improvement of large-scale photonic circuit integration, optoelectronic devices are increasingly integrated on silicon-based platforms, such as modulators, optical switches, and lasers [1–5]. However, with the increased popularity of on-chip devices, the transmission and coupling losses between devices have become an increasingly serious problem; as such, there is an urgent need for high-efficiency chip-scale amplifiers to compensate for these losses [6–8].

Er-doped fiber amplifiers and lasers have achieved great success in long-distance optical communication systems in recent decades [9, 10]. However, high-performance chip-scale integrated optical applications require Er-based materials with much higher gain. In general, chip-scale Er-based amplifiers adopt Al_2O_3 as the parent material because of its high solid solubility, compatibility with CMOS technology, and appropriate refractive index. For example, Mu et al. [11] achieved an on-chip gain of 10 dB by depositing Er-doped Al_2O_3 on a low-loss 5.9-cm-long silicon nitride waveguide. In addition, Sun et al. [12] deposited Al_2O_3 in a slot waveguide using atomic layer deposition (ALD), thereby concentrating the optical mode

* Corresponding author (email: xjwang@pku.edu.cn)

in the gain material in the slot and achieving a net gain of 20 dB · cm^{-1}. Alternatively, Er-doped Al_2O_3 has also been utilized as the gain medium for on-chip lasers, as demonstrated by Purnawirman et al. [13] for a 1.53-μm-wavelength laser, achieving an output power of 5.43 mW and a linewidth of 5.3 kHz.

Despite the achievements of Er-doped waveguide amplifiers, they retain an intrinsic deficiency in that the maximum achievable Er doping concentration is 10^{20} cm^{-3} owing to its limited solid solubility, which makes improving the material gain difficult. In contrast, in erbium silicate-based materials, Er^{3+} exists as a compound cation, which overcomes the solid solubility and allows Er doping concentrations as high as 10^{22} cm^{-3} to be achieved [14]. In 2017, Ning et al. [15] prepared single-crystal Er chlorosilicate nanowires and reported a gain of more than 100 dB · cm^{-1} at a wavelength of 1.53 μm. However, the small diameter and short length of the nanowires make them hard to integrate with other on-chip optoelectronic devices. Therefore, thin films remain the principal method for preparing on-chip waveguide devices. In addition, erbium silicate-based materials require annealing above 1000°C to crystallize and activate the Er^{3+}, which is too high for CMOS front-end processing and complicates large-scale on-chip integration [16,17]. Consequently, reducing the annealing temperature of erbium silicate materials is crucial for the effective integration of chip-scale amplifiers with other on-chip optoelectronic devices.

To address these issues, the addition of Bi_2O_3 to the gain material has been investigated as a strategy to reduce the crystallization temperature of the erbium silicate material, as the crystallization temperature and melting point of Bi_2O_3 are approximately 300°C and 800°C, respectively [18]. In addition, the presence of Bi^{3+} in the thin films can enhance the luminescence properties of Er^{3+}, which helps to improve the gain properties of the material [19–21].

Here, we report a low-fabrication-temperature, high-luminescence-efficiency gain material by adding Bi_2O_3 to the erbium-ytterbium silicate mixed film. The experimental results demonstrate that thin films with this composition can crystallize and be optically activated using an annealing temperature of 600°C, which is the lowest activation temperature of on-chip waveguide amplifier to our knowledge. To demonstrate the application potential of the proposed gain material, we used it as the basis for a chip-scale waveguide amplifier and analyzed its performance using a theoretical multi-energy-level model of Bi-Er-Yb in the mixed thin film. We achieved a maximum on-chip gain of 23 dB in a 3.3-mm-long waveguide under pump and signal powers of 300 mW and 1 μW, respectively. As such, we believe that the proposed gain material shows immense promise for the realization of on-chip amplifiers and lasers for large-scale nanophotonic integrated circuits.

2 Materials and methods

The erbium-ytterbium silicate thin films incorporating Bi_2O_3 were deposited on SiO_2 substrates via magnetron sputtering. The Bi_2O_3 and erbium-ytterbium silicate targets were sputtered alternately at a pressure of 1 Pa in an Ar atmosphere. To improve the quality of the films, the substrates were rotated at a speed of 20 r · min^{-1} to improve the surface uniformity. The radio frequency power applied to the two targets was 200 W, and the ratio of the Bi_2O_3 and erbium-ytterbium silicate concentrations was controlled by adjusting the deposition time of the two targets. The ratio of the components in the erbium-ytterbium silicate target used in the experiment was Er_2O_3:Yb_2O_3:SiO_2 = 1:5:20, which has been shown to enhance the photoluminescence (PL) intensity, as described in our previous work [22]. Subsequently, the mixed thin films were annealed in an air environment at temperatures ranging from 600°C to 1200°C to induce the formation of an $Er_2Si_2O_7$ lattice structure, which is considered a desirable lattice structure for chip-scale amplifiers and lasers [23–25].

Two measurement systems were used to extract and confirm the optical characteristics of the mixed thin films. The PL intensity was studied using a 980-nm-wavelength laser as the pump, while the lattice structures of the films were analyzed using X-ray diffraction (XRD) with Cu K_α radiation.

3 Results and discussion

3.1 Optical property measurements

Figure 1 shows the PL spectra of films possessing Bi to Er-Yb concentration ratios ranging from 0 to 1.4, and annealing temperatures ranging from 600°C to 1200°C. There was no PL spectrum detected under any Bi to Er-Yb concentration ratios when the annealing temperature was below 600°C. The inset shows

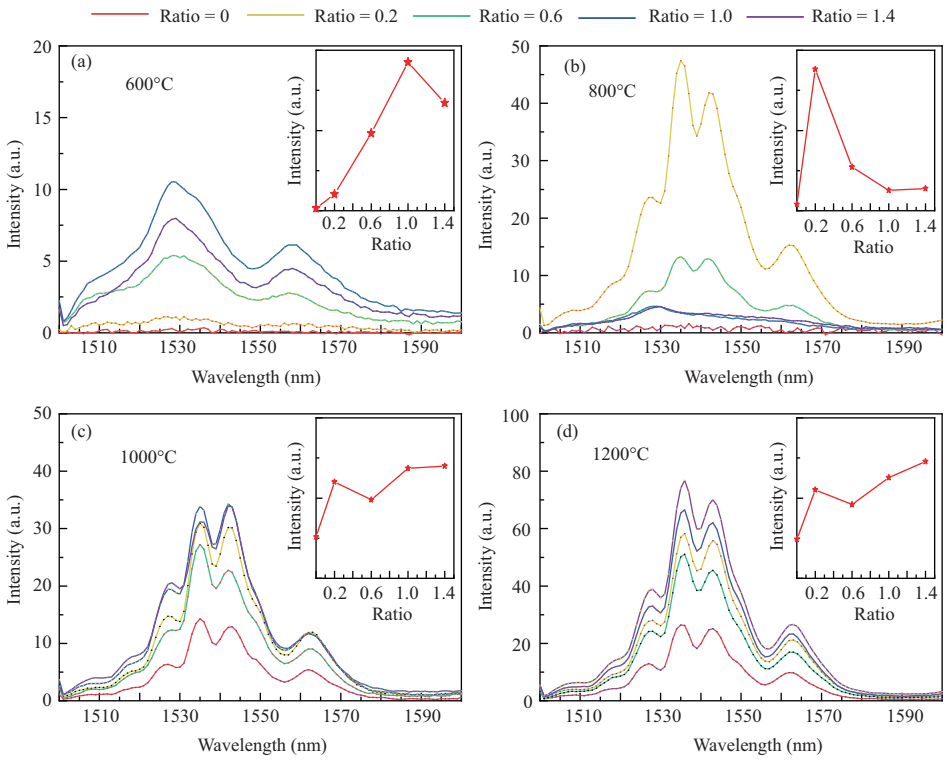

Figure 1 Photoluminescence spectra of different concentration ratios of Bi_2O_3 and erbium-ytterbium silicate mixed films for annealing temperatures of (a) 600°C, (b) 800°C, (c) 1000°C, and (d) 1200°C. The insets show the variation of the PL integral intensity for the different film compositions at the corresponding annealing temperature.

the variation in the PL integral intensity of the different film compositions at the corresponding annealing temperature. As shown in Figure 1(a), at an annealing temperature of 600°C and no Bi_2O_3 component in the film, no PL response was measured, with PL behavior only emerging following the introduction of Bi_2O_3. This is attributed to the change in the crystalline state of the material following the addition of Bi_2O_3. In addition, as the Bi_2O_3 concentration increases, the PL intensity of the films increases initially, reaching a maximum at a concentration ratio of 1, before gradually beginning to reduce. As shown in Figure 1(b), at an annealing temperature of 800°C, the PL response is similarly absent prior to the introduction of Bi_2O_3. However, in this case, the maximum PL intensity corresponds to a lower Bi_2O_3 concentration ration of 0.2 and decreases as the ratio increases. As shown in Figures 1(c) and (d), for annealing temperatures at or exceeding 1000°C, PL spectra are obtained without the addition of Bi_2O_3, and although adding Bi_2O_3 increases the PL intensity, the precise concentration of Bi_2O_3 has a less pronounced impact than at lower annealing temperatures.

To understand the variation in the PL spectra at different annealing temperatures, the lattice structures of the mixed films were analyzed using XRD. Figures 2(a) and (b) show the XRD patterns of Bi_2O_3 films and erbium-ytterbium silicate films, respectively, at annealing temperatures ranging from 600°C to 1200°C. At 600°C, the XRD peaks of the Bi_2O_3 film agree closely with the Bi_2O_3 reference structure (JCPDS 72-0398), indicating that the film can crystallize under these conditions. However, at 800°C, only four of the original nine peaks remain, while a single peak remains for annealing at or above 1000°C, which is due to the low melting point of Bi_2O_3 (800°C). At an annealing temperature of 800°C, the Bi_2O_3 film was partially melted causing the lattice structure deteriorated. Above 1000°C, the Bi_2O_3 film was almost completely melted, resulting in the almost complete disappearance of peaks in the XRD pattern. As shown in Figure 2(b), the erbium-ytterbium silicate films could not crystallize when annealed below 1000°C. It is not certain whether the peak at 33° is due to the crystallization of SiO_2 in the substrate or the erbium-ytterbium silicate film. For annealing above 1000°C, the XRD peaks are consistent with the characteristic $Yb_2Si_2O_7$ structure (JCPDS 25-1345), which proves that the erbium-ytterbium silicate film needs to be annealed above 1000°C to ensure a crystalline structure. In addition, because Yb accounts for a greater proportion of the erbium-ytterbium silicate films than Er, the measured XRD peaks are closer to the lattice structure of $Yb_2Si_2O_7$ than that of $Er_2Si_2O_7$.

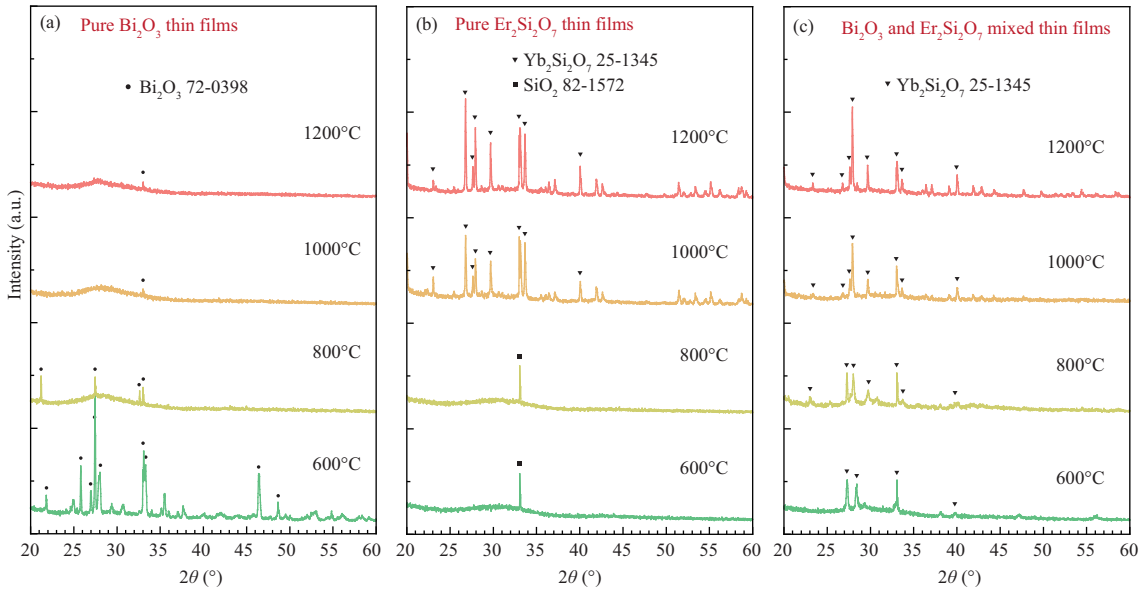

Figure 2 XRD patterns of (a) Bi_2O_3, (b) erbium-ytterbium silicate and (c) Bi_2O_3 and erbium-ytterbium silicate mixed thin films at different annealing temperatures.

Figure 2(c) shows the XRD pattern of the Bi_2O_3 and erbium-ytterbium silicate mixed film at annealing temperatures ranging from 600°C to 1200°C. At 600°C, the XRD pattern has three main peaks, located at 27°, 28°, and 33°, which are consistent with the XRD pattern of erbium-ytterbium silicate. This proves that the mixed thin film formed a lattice structure which is similar to erbium-ytterbium silicate. Moreover, as the annealing temperature increases from 800°C to 1200°C, the XRD pattern exhibits additional peaks and more closely resembles the pattern of erbium-ytterbium silicate. This is completely different from the crystallization process of Bi_2O_3 films. On the contrary, it is more consistent with the crystallization process of erbium-ytterbium silicate films. These results suggest that the Bi_2O_3 and erbium-ytterbium silicate mixed thin film can crystalize at 600°C and has a similar lattice structure to an erbium-ytterbium silicate thin film. In addition, as the annealing temperature increases, the crystallinity improves and the lattice structure approaches that of an erbium-ytterbium silicate thin film. These results prove that the addition of Bi_2O_3 can reduce the crystallization temperature of the erbium-ytterbium silicate mixed film, most likely owing to the low crystallization temperature of Bi_2O_3.

The XRD patterns help to elucidate the variation in the PL spectra. Crystallization at an annealing temperature of 600°C was realized only after the introduction of Bi_2O_3, with crystallization essential to elicit a PL response from the erbium-ytterbium silicate mixed films. In addition, the PL intensities are related to the concentration ratio of the film components, which may be because the Bi^{3+} ions in the mixed thin films increased the separation between Er^{3+} ions. As the Bi^{3+} content increases, the concentration quenching effect of the Er^{3+} ions is increasingly suppressed, thus enhancing the luminescent effect of Er^{3+}. Nevertheless, when the concentration ratio is excessively high, the Er^{3+} concentration is too low, resulting in a decreased PL intensity. As shown in Figure 1, a concentration ratio of 1 yielded an impressive PL intensity at all annealing temperatures other than 800°C, where a lower concentration ratio produced the strongest PL response. This behavior is attributed to the low melting point of Bi_2O_3. The results indicate that partially melted Bi_2O_3 can decrease the PL intensity, with the impact becoming more pronounced as the Bi_2O_3 content increases. For annealing above 1000°C, the erbium-ytterbium silicate film was able to crystallize without any difficulty, giving rise to PL spectra. Above 1000°C, most of the Bi_2O_3 in the Bi_2O_3 and erbium-ytterbium silicate mixed films melts, which leads to small changes in the PL intensities of the films as the concentration ratio increases; however, most importantly, the PL intensities are all higher than that of erbium-ytterbium silicate, indicating that the addition of Bi_2O_3 can enhance the luminescent effect of Er^{3+} ions.

3.2 Chip-scale waveguide amplifier design

The erbium-ytterbium silicate and Bi_2O_3 mixed thin film can crystallize, activate the Er^3+ ions, and realize high PL efficiency at an annealing temperature of 600°C, which is compatible with CMOS front-

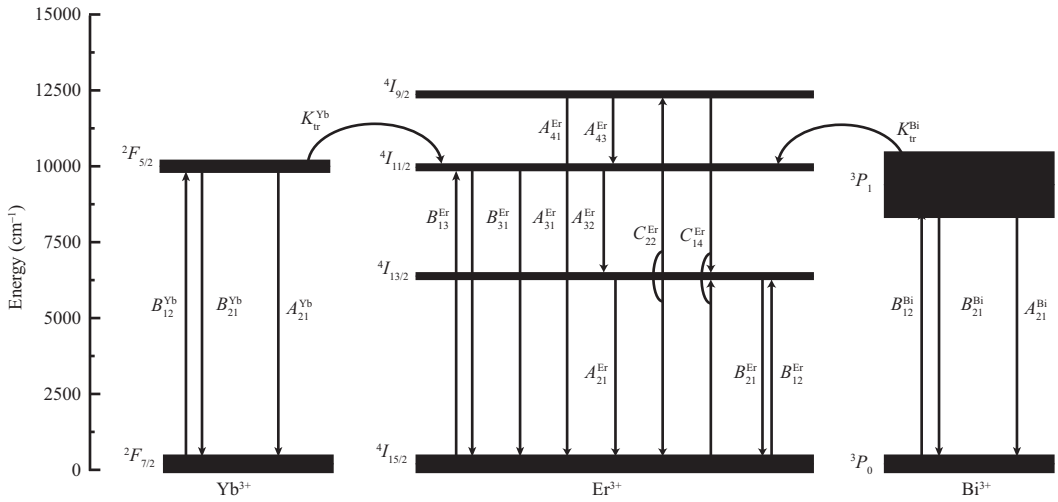

Figure 3 Energy level structure of Er^{3+}, Yb^{3+}, and Bi^{3+}, and the corresponding electronic transition processes.

end processing and facilitates large-scale integration with other optoelectronic devices. To analyze the PL property and the signal enhancement effect of the mixed thin film in greater depth, an accurate and systematic model of the Bi-Er-Yb multi-energy-level structure is established [26]. Figure 3 shows the multi-energy-level structure of Er^{3+}, Yb^{3+}, Bi^{3+}, and the corresponding electronic transition processes. In Bi_2O_3 and erbium-ytterbium silicate mixed thin films, the Yb^{3+} and Bi^{3+} ions absorb pump power and transfer the energy to the Er^{3+} ions. As such, Yb^{3+} and Bi^{3+} adopt two-level models that include the stimulated absorption and radiation of the pump (B_{12}^{Yb}, B_{21}^{Yb}, B_{12}^{Bi}, B_{21}^{Bi}), the spontaneous radiation (A_{21}^{Yb}, A_{21}^{Bi}), and the process of energy transfer to Er^{3+} ($K_{\mathrm{tr}}^{\mathrm{Yb}}$, $K_{\mathrm{tr}}^{\mathrm{Bi}}$). A four-energy-level model of Er^{3+} was established, including the stimulated absorption and radiation of the pump (B_{13}^{Er}, B_{31}^{Er}), the stimulated absorption and radiation of the signal (B_{12}^{Er}, B_{21}^{Er}), the spontaneous emission (A_{41}^{Er}, A_{43}^{Er}, A_{31}^{Er}, A_{32}^{Er}, A_{21}^{Er}), the cooperative up-conversion (C_{22}^{Er}), and the cross relaxation (C_{14}^{Er}).

The electronic transition processes shown in Figure 3 satisfy the following equations.

Er^{3+} energy level equation:

$$\begin{cases} \dfrac{\partial N_1^{\mathrm{Er}}}{\partial t} = B_{31}^{\mathrm{Er}} N_3^{\mathrm{Er}} - B_{13}^{\mathrm{Er}} N_1^{\mathrm{Er}} + A_{31}^{\mathrm{Er}} N_3^{\mathrm{Er}} + A_{41}^{\mathrm{Er}} N_4^{\mathrm{Er}} + A_{21}^{\mathrm{Er}} N_2^{\mathrm{Er}} + B_{21}^{\mathrm{Er}} N_2^{\mathrm{Er}} - B_{12}^{\mathrm{Er}} N_1^{\mathrm{Er}} \\ \qquad + C_{22}^{\mathrm{Er}} N_2^{\mathrm{Er}^2} - C_{14}^{\mathrm{Er}} N_1^{\mathrm{Er}} N_4^{\mathrm{Er}} - K_{\mathrm{tr}}^{\mathrm{Yb}} N_2^{\mathrm{Yb}} N_1^{\mathrm{Er}} - K_{\mathrm{tr}}^{\mathrm{Bi}} N_2^{\mathrm{Bi}} N_1^{\mathrm{Er}} = 0, \\ \dfrac{\partial N_2^{\mathrm{Er}}}{\partial t} = B_{12}^{\mathrm{Er}} N_1^{\mathrm{Er}} - B_{21}^{\mathrm{Er}} N_2^{\mathrm{Er}} + A_{32}^{\mathrm{Er}} N_3^{\mathrm{Er}} - A_{21}^{\mathrm{Er}} N_2^{\mathrm{Er}} - 2C_{22}^{\mathrm{Er}} N_2^{Er2} + 2C_{14}^{\mathrm{Er}} N_1^{\mathrm{Er}} N_4^{\mathrm{Er}} = 0, \\ \dfrac{\partial N_3^{\mathrm{Er}}}{\partial t} = B_{13}^{\mathrm{Er}} N_1^{\mathrm{Er}} - B_{31}^{\mathrm{Er}} N_3^{\mathrm{Er}} - A_{31}^{\mathrm{Er}} N_3^{\mathrm{Er}} - A_{32}^{\mathrm{Er}} N_3^{\mathrm{Er}} + A_{43}^{\mathrm{Er}} N_4^{\mathrm{Er}} + K_{\mathrm{tr}}^{\mathrm{Yb}} N_2^{\mathrm{Yb}} N_1^{\mathrm{Er}} \\ \qquad + K_{\mathrm{tr}}^{\mathrm{Bi}} N_2^{\mathrm{Bi}} N_1^{\mathrm{Er}} = 0, \\ \dfrac{\partial N_4^{\mathrm{Er}}}{\partial t} = -A_{41}^{\mathrm{Er}} N_4^{\mathrm{Er}} - A_{43}^{\mathrm{Er}} N_4^{\mathrm{Er}} + C_{22}^{\mathrm{Er}} N_2^{\mathrm{Er}^2} - C_{14}^{\mathrm{Er}} N_1^{\mathrm{Er}} N_4^{\mathrm{Er}} = 0, \end{cases} \tag{1}$$

and

$$N_1^{\mathrm{Er}} + N_2^{\mathrm{Er}} + N_3^{\mathrm{Er}} + N_4^{\mathrm{Er}} = N_{\mathrm{total}}^{\mathrm{Er}}\,, \tag{2}$$

where N_1^{Er}, N_2^{Er}, N_3^{Er} and N_4^{Er} indicate the concentration of Er^{3+} at each energy level and $N_{\mathrm{total}}^{\mathrm{Er}}$ indicates the total Er^{3+} concentration.

Yb^{3+} energy level equation:

$$\begin{cases} \dfrac{\partial N_1^{\mathrm{Yb}}}{\partial t} = B_{21}^{\mathrm{Yb}} N_2^{\mathrm{Yb}} - B_{12}^{\mathrm{Yb}} N_1^{\mathrm{Yb}} + A_{21}^{\mathrm{Yb}} N_2^{\mathrm{Yb}} + K_{\mathrm{tr}}^{\mathrm{Yb}} N_2^{\mathrm{Yb}} N_1^{\mathrm{Er}} = 0, \\ \dfrac{\partial N_2^{\mathrm{Yb}}}{\partial t} = B_{12}^{\mathrm{Yb}} N_1^{\mathrm{Yb}} - B_{21}^{\mathrm{Yb}} N_2^{\mathrm{Yb}} - A_{21}^{\mathrm{Yb}} N_2^{\mathrm{Yb}} - K_{\mathrm{tr}}^{\mathrm{Yb}} N_2^{\mathrm{Yb}} N_1^{\mathrm{Er}} = 0, \end{cases} \tag{3}$$

Table 1 Parameters used in the Bi_2O_3 and erbium-ytterbium silicate mixed film model

Parameter	Symbol	Value
Signal wavelength	λ_s	1530 nm
Pump wavelength	λ_p	980 nm
Total concentration	N_{total}	$(2.8-3.9)\times10^{22}$ cm^{-3}
Er^{3+} radiation lifetime at $^4I_{11/2}$	τ_{31}^{Er}	100 μs
Er^{3+} non-radiation lifetime at $^4I_{11/2}$	τ_{32}^{Er}	100 μs
Er^{3+} radiation lifetime at $^4I_{9/2}$	τ_{41}^{Er}	1 μs
Er^{3+} non-radiation lifetime at $^4I_{9/2}$	τ_{43}^{Er}	1 μs
Yb^{3+} radiation lifetime at $^2F_{5/2}$	τ_{21}^{Yb}	2 ms
Bi^{3+} radiation lifetime at $^3P_1$	τ_{21}^{Bi}	400 μs
Er^{3+} absorption cross section at 980 nm	σ_{13}^{Er}	2.58×10^{-21} cm^2
Er^{3+} emission cross section at 980 nm	σ_{31}^{Er}	2.58×10^{-21} cm^2
Yb^{3+} absorption cross section at 980 nm	σ_{12}^{Yb}	1.2×10^{-20} cm^2
Yb^{3+} emission cross section at 980 nm	σ_{21}^{Yb}	1.2×10^{-20} cm^2
Bi^{3+} absorption cross section at 980 nm	σ_{12}^{Bi}	2×10^{-20} cm^2
Bi^{3+} emission cross section at 980 nm	σ_{21}^{Bi}	2×10^{-20} cm^2
Er^{3+} absorption cross section at 1530 nm	σ_{12}^{Er}	1.24×10^{-20} cm^2
Er^{3+} emission cross section at 1530 nm	σ_{21}^{Er}	1.24×10^{-20} cm^2
Er^{3+} cooperative upconversion coefficient	C_{22}^{Er}	1×10^{-16} cm$^3\cdot$ s^{-1}
Er^{3+} cross-relaxation coefficient	C_{14}^{Er}	1×10^{-15} cm$^3\cdot$ s^{-1}
Yb^{3+} energy transfer coefficient	$K_{\text{tr}}^{\text{Yb}}$	1×10^{-16} cm$^3\cdot$ s^{-1}
Bi^{3+} energy transfer coefficient	$K_{\text{tr}}^{\text{Bi}}$	1×10^{-16} cm$^3\cdot$ s^{-1}

and

$$N_1^{\text{Yb}}+N_2^{\text{Yb}}=N_{\text{total}}^{\text{Yb}}\,, \tag{4}$$

where N_1^{Yb} and N_2^{Yb} indicate the concentration of Yb^{3+} at each energy level and $N_{\text{total}}^{\text{Yb}}$ indicates the total Yb^{3+} concentration.

Bi^{3+} energy level equation:

$$\begin{cases}\dfrac{\partial N_1^{\text{Bi}}}{\partial t}=B_{21}^{\text{Bi}}N_2^{\text{Bi}}-B_{12}^{\text{Bi}}N_1^{\text{Bi}}+A_{21}^{\text{Bi}}N_2^{\text{Bi}}+K_{\text{tr}}^{\text{Bi}}N_2^{\text{Bi}}N_1^{\text{Er}}=0,\\ \dfrac{\partial N_2^{\text{Bi}}}{\partial t}=B_{12}^{\text{Bi}}N_1^{\text{Bi}}-B_{21}^{\text{Bi}}N_2^{\text{Bi}}-A_{21}^{\text{Bi}}N_2^{\text{Bi}}-K_{\text{tr}}^{\text{Bi}}N_2^{\text{Bi}}N_1^{\text{Er}}=0,\end{cases} \tag{5}$$

and

$$N_1^{\text{Bi}}+N_2^{\text{Bi}}=N_{\text{total}}^{\text{Yb}}\,, \tag{6}$$

where N_1^{Bi} and N_2^{Bi} indicate the concentration of Bi^{3+} at each energy level and $N_{\text{total}}^{\text{Bi}}$ indicates the total Bi^{3+} concentration.

In the above equations, $A_{ij}=1/\tau_{ij}$, where τ_{ij} is the spontaneous emission lifetime, and $B_{ij}=(\sigma_{ij}/(A_c h\nu))P$, where σ_{ij} is the absorption or emission cross section between energy levels i and j. Furthermore, P denotes the power of the signal or pump, A_c represents the optical mode area, h is the Planck constant, and ν is the frequency of the signal or pump.

According to the above expressions, the electron concentration of each energy level of Er^{3+}, Yb^{3+}, and Bi^{3+} can be solved under the corresponding power of the signal and pump. Thus, the PL intensity at 1530 nm can be calculated as [27]

$$P_{\text{PL}}\propto\frac{N_2^{\text{Er}}P_{\text{pump}}\tau_{21}^{\text{Er}}}{h\nu_{\text{pump}}}, \tag{7}$$

where τ_{21}^{Er} can be measured experimentally. Table 1 summarizes the parameters used in the modeling.

The PL intensities of mixed films with different concentration ratios fabricated using an annealing temperature of 600°C were calculated using the parameters listed in Table 1 and for a pump wavelength of 1530 nm and compared with the experimental results, with the results shown in Figure 4. The inset shows the measured luminescence lifetime (τ_{21}^{Er}) at 1530 nm, which is 1.36 ms. The simulation results (red line) show that as the concentration ratio increases, the PL intensities at 1530 nm first increase and then

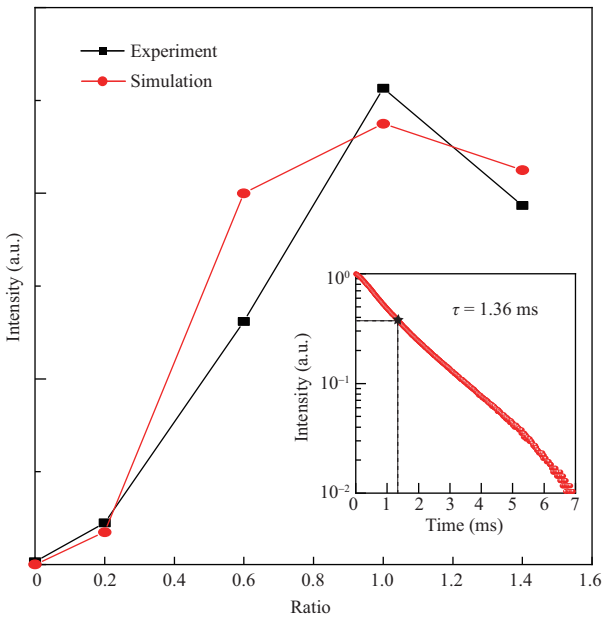

Figure 4 Comparison of experimental and simulated PL intensities at a pump wavelength of 1530 nm for mixed films (annealed at 600°C) with different concentration ratios. The inset shows the 1530 nm luminescence lifetime measured in the experiment.

decrease, with the peak PL intensity corresponding to a concentration ratio of 1, which corroborates the experiment results (black line). These results confirm the accuracy of our energy-level structure model for the mixed thin films.

Next, we designed a chip-scale waveguide amplifier based on the mixed thin-film gain material, with the structure prepared on a SiO_2 substrate and surrounded by SiO_2 cladding, as shown in Figure 5. The strip waveguide consists of the Bi_2O_3 and erbium-ytterbium silicate mixed material, with the width and height of the waveguide both set to 1 μm. The refractive index of the erbium-ytterbium silicate mixed material is approximately 2. The thickness of the substrate and the cladding is both above 5 μm, which can ensure the optical mode restricted in the strip waveguide. The restriction factors of the pump and signal are 96.9% and 91.3%, respectively, with their similar mode distributions benefitting the enhancement of the signal gain of the chip-scale waveguide amplifier.

The absorption and gain coefficients of the pump and signal in the waveguide can be solved using the following transmission equations:

$$\begin{cases} \dfrac{\mathrm{d}P_p(z)}{\mathrm{d}z} = \left(\sigma_{31}^{\mathrm{Er}} N_3^{\mathrm{Er}} - \sigma_{13}^{\mathrm{Er}} N_1^{\mathrm{Er}} + \sigma_{21}^{\mathrm{Yb}} N_2^{\mathrm{Yb}} - \sigma_{12}^{\mathrm{Yb}} N_1^{\mathrm{Yb}} + \sigma_{21}^{\mathrm{Bi}} N_2^{\mathrm{Bi}} - \sigma_{12}^{\mathrm{Bi}} N_1^{\mathrm{Bi}} - \alpha\right) \Gamma_p P_p(z), \\ \dfrac{\mathrm{d}P_s(z)}{\mathrm{d}z} = \left(\sigma_{21}^{\mathrm{Er}} N_2^{\mathrm{Er}} - \sigma_{12}^{\mathrm{Er}} N_1^{\mathrm{Er}} - \alpha\right) \Gamma_s P_s(z), \end{cases} \tag{8}$$

where α is the transmission loss (considered to be 3 dB $\cdot$ cm^{-1}) and Γ_p and Γ_s are the pump and signal restriction factors, respectively.

Figure 5(b) shows the signal gain of the chip-scale waveguide amplifier as a function of the waveguide propagation distance when the signal power is fixed at 1 μW, the pump power varies from 100 to 500 mW, and the concentration ratio of the amplifier material is 1, which corresponds to the optimal concentration ratio determined via the experiments. When the signal power varies around 1 μW, the gain curves are basically unchanged. As the propagation distance increases, the signal gain increases uninterrupted to the maximum value, before decreasing owing to the absorption and transmission losses of the pump power. The loss of the pump power is reduced at shorter transmission distances, which supports population inversion in the waveguide amplifier. As the propagation distance increases, most of the pump power is absorbed and dissipated, with the residual pump power insufficient to induce population inversion. Therefore, the optimal length of the waveguide amplifier corresponds to the pump power required to achieve population inversion. For a pump power of 500 mW, the optimal waveguide length is 3.5 mm, resulting in a signal gain of 24.3 dB.

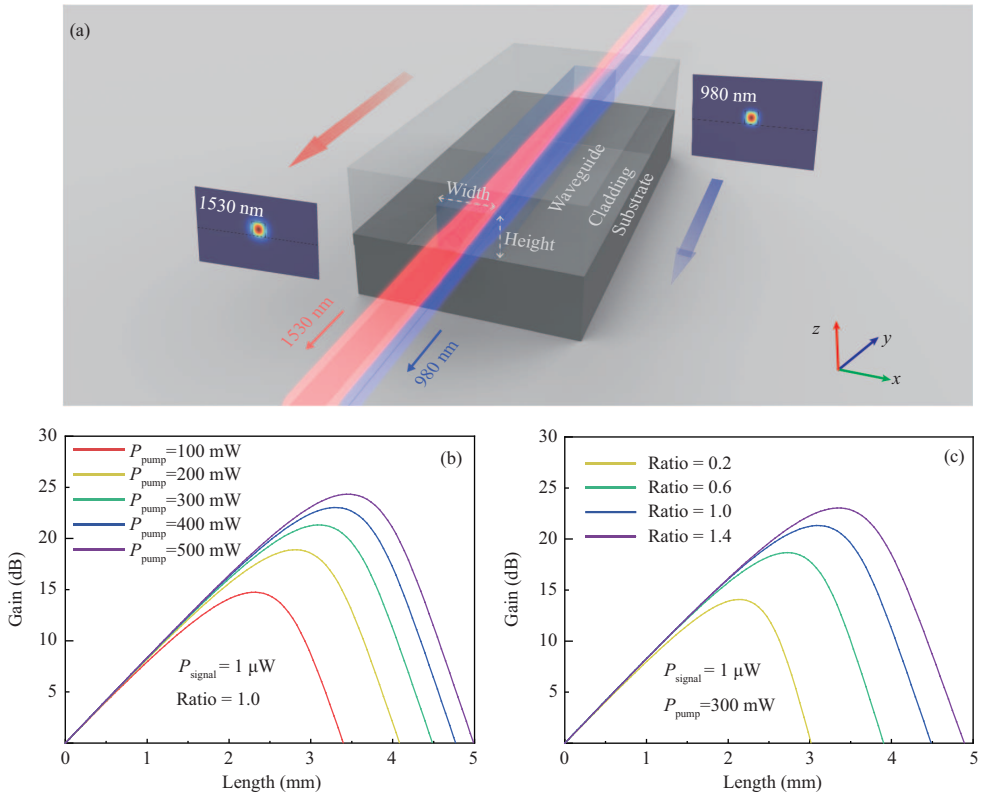

Figure 5 (a) Diagram of the chip-scale waveguide amplifier structure. The strip waveguide comprises the Bi_2O_3 and erbium-ytterbium silicate mixed material. The substrate and cladding are both SiO_2. (b) Signal gain at different transmission distances as the pump power is increased from 100 to 500 mW (signal power: 1 μW, concentration ratio: 1). (c) Signal gain at different transmission distances as the concentration ratio is increased from 0 to 1.4 (signal power: 1 μW, pump power: 300 mW).

Figure 5(c) shows the signal gain of waveguide amplifiers in which the concentration ratio of the amplifier material varies from 0.2 to 1.4 under different transmission distances for a pump power of 300 mW and a signal power of 1 μW. Up to a transmission distance of 2 mm, as the transmission distance increases, the signal gain increases continuously and is largest when the concentration ratio is 1. At longer transmission distances, the signal gain gradually reaches a peak value and then begins decreasing. In addition, when the concentration ratio is higher, the concentration of Er^{3+} in the film is lower and the absorption coefficient of the pump power is lower; thus, the maximum transmission distance is longer and the maximum signal gain coefficient is larger. For a concentration ratio is 1.4, the optimal waveguide length is 3.3 mm. Under these conditions, the maximum signal gain can reach 23 dB. These results prove that the mixed thin film material demonstrates great promise for fabricating high-efficiency chip-scale amplifiers and lasers.

4 Conclusion

We demonstrate the low-temperature fabrication of a high-luminescence-efficiency gain material for chip-scale waveguide amplifiers based on Bi_2O_3 and erbium-ytterbium silicate mixed thin films. A crystalline lattice structure coupled with a relatively high PL intensity was achieved by annealing the mixed films at 600°C. Owing to the low annealing temperature, the proposed amplifier material has great potential for integration with other on-chip optoelectronic devices. We used the Bi_2O_3 and erbium-ytterbium silicate mixed thin film as the basis for a chip-scale waveguide amplifier. Under pump and signal powers of 300 mW and 1 μW, respectively, a peak on-chip gain of 23 dB was achieved using a waveguide length of 3.3 mm. These results prove that Bi_2O_3 and erbium-ytterbium silicate mixed thin films are promising candidates for the realization of on-chip amplifiers and lasers for large-scale nanophotonic integrated circuits.

Acknowledgements This work was supported by National Natural Science Foundation of China (Grant No. 61635001).

References

1 Atabaki A H, Moazeni S, Pavanello F, et al. Integrating photonics with silicon nanoelectronics for the next generation of systems on a chip. Nature, 2018, 556: 349–354
2 Thomson D, Zilkie A, Bowers J E, et al. Roadmap on silicon photonics. J Opt, 2016, 18: 073003
3 Bogaerts W, Pérez D, Capmany J, et al. Programmable photonic circuits. Nature, 2020, 586: 207–216
4 Li N, Xin M, Su Z, et al. A silicon photonic data link with a monolithic erbium-doped laser. Sci Rep, 2020, 10: 1114
5 Hayat A, Tong J H, Chen C, et al. Multi-wavelength colloidal quantum dot lasers in distributed feedback cavities. Sci China Inf Sci, 2020, 63: 182401
6 Zimmerman D R, Spiekman L H. Amplifiers for the masses: EDFA, EDWA, and SOA amplets for metro and access applications. J Lightwave Technol, 2004, 22: 63–70
7 Liang D, Bowers J E. Recent progress in lasers on silicon. Nat Photon, 2010, 4: 511–517
8 Zhou P Q, Wang B, Wang X J, et al. Design of an on-chip electrically driven, position-adapted, fully integrated erbium-based waveguide amplifier for silicon photonics. OSA Continuum, 2021, 4: 790–814
9 Pu G Q, Zhang L, Hu W S, et al. Automatic mode-locking fiber lasers: progress and perspectives. Sci China Inf Sci, 2020, 63: 160404
10 Xi Q, Wei S H, Yuan C Z, et al. Experimental observation of coherent interaction between laser and erbium ions ensemble doped in fiber at sub 10 mk. Sci China Inf Sci, 2020, 63: 180505
11 Mu J, Dijkstra M, García-Blanco S M. Monolithic integration of Al_2O_3:Er^{3+} amplifiers in Si_3N_4 technology. In: Proceedings of European Conference on Lasers and Electro-Optics (CLEO Europe), 2019. 38
12 Rönn J, Zhang W W, Autere A, et al. Ultra-high on-chip optical gain in erbium-based hybrid slot waveguides. Nat Commun, 2019, 10: 432
13 Purnawirman, Li N, Magden E S, et al. Ultra-narrow-linewidth Al_2O_3:Er^{3+} lasers with a wavelength-insensitive waveguide design on a wafer-scale silicon nitride platform. Opt Express, 2017, 25: 13705–13713
14 Miritello M, Savio R L, Iacona F, et al. Efficient luminescence and energy transfer in erbium silicate thin films. Adv Mater, 2007, 19: 1582–1588
15 Sun H, Yin L, Liu Z, et al. Giant optical gain in a single-crystal erbium chloride silicate nanowire. Nat Photon, 2017, 11: 589–593
16 Mariani M, Possémé N. Front-End Processes. Nanoelectronics: Materials, Devices, Applications, 2017, 11
17 Colombeau B, Yeong S H, Tan D, et al. Ultra-shallow junction formation-physics and advanced technology. In: Proceedings of AIP Conference, 2008. 1066: 11
18 Shen Y D, Li Y W, Li W M, et al. Growth of Bi_2O_3 ultrathin films by atomic layer deposition. J Phys Chem C, 2012, 116: 3449–3456
19 Peng M, Zhang N, Wondraczek L, et al. Ultrabroad NIR luminescence and energy transfer in Bi and Er/Bi co-doped germanate glasses. Opt Express, 2011, 19: 20799
20 Xiao J, Cao J, Wang Y, et al. Temperature dependent energy transfer in Bi/Er codoped barium gallogermanate glasses for tunable and broadband NIR emission. J Mater Chem C, 2019, 7: 10544–10550
21 Dai N, Xu B, Jiang Z, et al. Effect of Yb^3+ concentration on the broadband emission intensity and peak wavelength shift in Yb/Bi ions co-doped silica-based glasses. Opt Express, 2010, 18: 18642–18648
22 Zhou P Q, Wang X J, He Y D, et al. Effect of deposition mechanisms on the infrared photoluminescence of erbium-ytterbium silicate films under different sputtering methods. J Appl Phys, 2019, 125: 175114
23 Wang X J, Nakajima T, Isshiki H, et al. Fabrication and characterization of Erbium silicates on SiO_2/Si substrates. Appl Phys Lett, 2009, 95: 041906
24 Miritello M, Savio R L, Iacona F, et al. Synthesis and luminescence properties of erbium silicate thin films. Mater Sci Eng-B, 2008, 146: 29–34
25 Savio R L, Miritello M, Piro A M, et al. The influence of stoichiometry on the structural stability and on the optical emission of erbium silicate thin films. Appl Phys Lett, 2008, 93: 021919
26 Zhou P Q, Wang S, Wang X J, et al. High-gain erbium silicate waveguide amplifier and a low-threshold, high-efficiency laser. Opt Express, 2018, 26: 16689
27 van den Hoven G N, Snoeks E, Polman A, et al. Photoluminescence characterization of Er-implanted Al_2O_3 films. Appl Phys Lett, 1993, 62: 3065–3067